Polymer 51 (2010) 3173–3180

Contents lists available at ScienceDirect

Polymer

journal homepage: www.elsevier.com/locate/polymer

In situ preparation of nano ZnO/hyperbranched polyimide hybrid film and their optical properties

Hong Gao [a], Daisuke Yorifuji [a], Junji Wakita [a], Zhen-Hua Jiang [b], Shinji Ando [a,*]

[a] Department of Chemistry and Materials Science, Tokyo Institute of Technology, 2-12-1-E4-5 Ookayama, Meguro-ku, Tokyo 152-8552, Japan
[b] Alan G. MacDiarmid Institute, College of Chemistry, Jilin University, Qianjin Street 2699, Changchun 130012, PR China

ARTICLE INFO

Article history:
Received 12 January 2010
Received in revised form
30 April 2010
Accepted 9 May 2010
Available online 15 May 2010

Keywords:
Hyperbranched polyimide
ZnO nanoparticles
Fluorescence

ABSTRACT

Novel hybrid films of fluorinated hyperbranched polyimide (HBPI) and zinc oxide (ZnO) were prepared via the *in situ* sol–gel polymerization technique, in which mono-ethanolamine (MEA) was used as the coupling agent between the termini of HBPI and the precursor of ZnO. The hybrid films were characterized by transmission electron microscopy (TEM), Fourier transform infrared (FT-IR) absorption, ultraviolet–visible (UV–vis) absorption, and fluorescent excitation/emission spectroscopy. The films, which originated from the colourless fluorinated HBPI structure and homogeneously dispersed ZnO nanoparticles, exhibited good optical transparency. Furthermore, two kinds of model compounds with and without ZnO and a HBPI film blended with ZnO microparticles were prepared to clarify the fluorescence mechanism in the pristine HBPI and *in situ* hybrid films. Efficient energy transfer from the ZnO nanoparticles to the aromatic HBPI main chains was observed in the *in situ* hybrid films, whereas energy transfer occurred only from the locally excited (LE) states to the charge-transfer (CT) state in the HBPI film. These facts demonstrate that the peripheral termini of HBPI are covalently bonded to ZnO particles via the MEA function, which operates as an effective pathway for energy transfer to give intense fluorescent emission.

1. Introduction

In past decades, there has been much progress in the growing field of semiconductor nanoparticle quantum dots (QDs) for light emitting diodes [1–3], new types of lasers [4], photovoltaic solar cells [5] and biolables [6]. Compared to the corresponding inorganic or polymeric components, polymer–inorganic hybrid materials usually allow one to couple advantages associated with the inorganic phase to polymers. Accordingly, the integration of inorganic nanoparticles into polymeric materials leads to a new class of functional materials [7]. Among the various metallic oxides, ZnO has been of great interest because of its wide band gap ($E_g = 3.36$ eV at room temperature) and high exciton binding energy ($E_b^{3D} \approx 0.06$ eV), which make ZnO a promising candidate for catalysts, sensors and optoelectronic devices [8–10].

Recently, aromatic polyimides (PIs) hybridized with metallic oxides created a new field of active research due to the unique combination of advantageous properties from each component, such as electrical, optical, mechanical and high thermal stability features [11]. Since the properties of hybrid films are significantly dependent on the conditions of inorganic nanoparticles, control of particle size, its distribution and dispersion homogeneity over the entire matrix is a critical prerequisite to assure the optical and electrical properties of nanohybrids for functional device applications [12].

Chemical hybridization methods based on the *in situ* sol–gel polymerization approach enables one to manipulate organic/inorganic interfacial interactions at the molecular level or on a nanometer scale, resulting in homogenous structures and thus overcoming the problem of nanoparticle agglomeration [13]. Whang et al. have developed *in situ* formation of PI–TiO_2 hybrid materials by using acetylacetone as the chelating agent to stabilize TiO_2 nanoparticles [12] and, very recently, transparent thin films of PI–TiO_2 nanohybrids have been successfully synthesized from a soluble PI with carboxylic acid end-groups by Chen et al. [14]. However, the development of synthetic methods or new processing techniques for integrating ZnO nanoparticles with PI without aggregation is still a challenging topic for a new class of optical and electronic materials.

In recent years, hyperbranched polymers have received increasing attention due to their better multi-functionalities arising from multiple end-groups, good solubility and gas separation

* Corresponding author. Tel./fax: +81 3 5734 2889.
E-mail address: sando@polymer.titech.ac.jp (S. Ando).

0032-3861/$ – see front matter © 2010 Elsevier Ltd. All rights reserved.
doi:10.1016/j.polymer.2010.05.019

ability, compared to linear type polymers having similar chemical structures [15]. In addition, a computer simulation study demonstrated that there are many open and accessible cavities which form from the periphery of neighboring branches in hyperbranched polymers [16]. Such a cavity can be considered as a kind of free volume hole, which is expected to increase optical transparency and liquid/gas solubilities, and to reduce the refractive index. For developing high-performance hybrid polymers, hyperbranched polyimides (HBPI)s may open a new route for organic/inorganic hybrid materials due to their unique chemical structure and physical properties. The large number of reactive groups at the periphery of HBPI offers a facile and straightforward way for further modification and specific applications [17–22]. Functionalization at the peripheral termini of HBPIs can be performed by reactions of end-groups with reagents containing certain functional groups.

HBPIs with CF_3 groups have been researched in our previous work [20]. It has been proved that the HBPIs containing $-CF_3$ groups exhibited excellent optical transparency in the visible region, which is beneficial for the study of fluorescence. To explore a new application of fluorine-containing HBPI as an optically transparent polymer matrix, we develop novel nanohybrid materials based on the HBPI in this study. We focus on the preparation of transparent ZnO/HBPI nanohybrid films via the *in situ* hybridization method to exploit the advantages of HBPIs. Difunctional mono-ethanolamine (MEA) was chosen to control the hydrolysis of the ZnO precursor, $(Zn(CH_3COO)_2)\cdot 2H_2O$ (ZAD), and it also functioned as a coupling agent between the ZnO nanoparticles and terminal anhydride groups of HBPI. The structure and composition of ZnO/HBPI hybrid films were characterized via transmission electron microscopy (TEM), Fourier transform infrared (FT-IR) absorption, UV/vis optical absorption and fluorescent excitation/emission spectroscopy. Furthermore, the optical properties and fluorescence mechanisms of ZnO/HBPI nanohybrid films were investigated in detail by comparing them with those of physically blended film and related model compounds.

2. Experimental

2.1. Materials

Zincacetate dianhydrate $(Zn(CH_3COO)_2)\cdot 2H_2O$ (ZAD) (99.0%) and mono-ethanolamine (MEA), purchased from Wako Pure Chemical Industry (Wako), were used without further purification. Phthalic anhydride, biphenyltetracarboxylic dianhydride (s-BPDA), purchased from Wako, was purified by sublimation under reduced pressure. *N*, *N*-Dimethylacetamide (DMAc, anhydrous, 99.8%), purchased from Aldrich, was dried with a molecular sieve prior to use.

2.2. Characterization

FT-IR absorption spectra were measured with a Thermo-Nicolet Avater-320 spectrometer equipped with a Thunderdome ATR attachment (IRE: Ge, incident angle: 45°). Far-infrared (Far-IR) spectra were measured with a JASCO FT-IR-6100 spectrometer in the range of 650–250 cm^{-1}. Differential scanning calorimetry (DSC) measurements were performed on a Shimadzu DSC-60 at a heating rate of 10 °C/min under nitrogen. Thermal gravimetric analyses (TGA) were performed on a Shimadzu DTG-60 in nitrogen and air atmospheres at a heating rate of 10 °C/min. Wide-angle X-ray diffraction (WAXD) measurements were performed using a Rigaku Mini Flex II diffractometer equipped with a CuK_α radiation source. Scanning was carried out on the equator in the 2θ range of 3°–80° at a scan speed of 1°/min. The UV–vis optical absorption spectra of PI films formed on fused silica substrates were measured with a Hitachi U-3500 spectrophotometer. A blank fused silica substrate was used as a reference. The fluorescence spectra of PI films were measured with a Hitachi F-4500 spectrophotometer using the front-face setup for reducing self-absorption. The photomultiplier tube of Hamamatsu R-928 was used without additional calibration for sensitivity dispersion. A transmission electron micrograph (TEM) equipped with an electron-dispersive X-ray spectroscopy (EDS analysis) (EDAX Inc.) was performed on a JEOL JEM-2010F.

2.3. Polymer synthesis

2.3.1. Synthesis of HBPI-MEA-ZnO

The synthesis of ZnO complexes was achieved by the hydrolysis of ZAD with MEA, as reported by Znaidi et al. [23]. A typical preparation procedure of an MEA-Zn^{2+} solution consists of the following steps. A Zn(II) solution (0.1 mol/L) was prepared by refluxing ZAD in ethanol at 80 °C for 2 h under continuous stirring. Subsequently, MEA was added to this solution. The molar ratios of MEA to Zn(II) were controlled as follows: 1:0.25, 1:1, 1:2. After stirring for an extra 24 h at room temperature, the solvent (ethanol) in the mixed solution was removed and replaced by 5 mL of DMAc using a rotary evaporator under vacuum. The polycondensation of HBPI-MEA-ZnO was successively carried out in a flask by adding dropwise a triamine 1,3,5-tris(2-trifluoromethyl-4-aminophenoxy) benzene (TFAPOB) (0.151 g, 0.25 mmol) solution into s-BPDA dianhydride (0.147 g, 0.5 mmol) in DMAc (6 mL) under a nitrogen flow at room temperature, followed by further stirring for 12 h to achieve an anhydride-terminated hyperbranched poly(amic acid) (PAA) solution. Various amounts of the MEA-Zn^{2+} solution were added dropwise to the PAA solution (with MEA: terminal anhydride groups = 1:1). They were further stirred for 48 h, and transparent solutions were thus obtained. The pristine and MEA-Zn^{2+} hybridized hyperbranched PAA solution was cast onto silicon and silica substrates, and then heated stepwise at 100, 150, 200 and 250 °C for 2 h at each temperature under nitrogen. FT-IR spectra confirmed that a thermal imidization reaction was almost completed after this curing process. The films were further treated at 300 °C for 1 h under air for formation of the ZnO nanoparticles formed in the HBPI films.

2.3.2. Preparation of HBPI-blend-ZnO

Sub-μm sized ZnO particles were prepared from an MEA-Zn^{2+} solution for the use of physical blending with a PAA solution. The ZnO powder was obtained by thermal deposition of an MEA-Zn^{2+} solution at around 400 °C and then annealed in air at 900 °C to accomplish thermal oxidation. The average size of the ZnO particles was estimated to be around 400 nm by FE-SEM microscope. Subsequently, the ZnO particles (0.03 g) were slowly added to a hyperbranched PAA solution which is same amount as that for chemical hybrid HBPI, and stirred for 48 h. The content of the ZnO particles was set at 10 wt%. The PAA-blend-ZnO solution was cast onto silicon and silica substrates, and thermally treated stepwise by the same procedure as that for HBPI-MEA-ZnO films.

2.4. Preparation of model compounds

2.4.1. Synthesis of model compound ***1***

Phthalic anhydride (PHAD) (0.74 g, 5 mmol) was dissolved in 4 mL of DMAc in a 50-mL three-necked flask with stirring under a nitrogen atmosphere. A 4 mL DMAc solution of MEA (0.306 g, 5 mmol) was slowly added dropwise through a syringe over 0.5 h. The reaction was further conducted for 12 h at room temperature. Subsequently, a mixture of triethylamine (1.0 g) and acetic anhydride (3.0 g) was added. The solution was kept at 40 °C for 12 h and then poured into iced water. The precipitated crude product of

compound **1** was collected by filtration and purified by sublimation under reduced pressure. Mp, 92 °C, ^{1}H NMR (400 MHz, $CDCl_3$-d_6, ppm) δ: 2.01 (1H, hydroxyl), 3.97 (2H, $-H_2-$), 4.28 (2H, $-H_2-$), 7.72 and 7.81 (4H, Ar-H of phthalic anhydride residue).

*2.4.2. Synthesis of model compound **2***

The synthetic method for compound **2** was the same as the compound **1** except that an MEA-Zn^{2+} solution was used instead of an MEA solution. An 4 mL DMAc solution of MEA-Zn^{2+} solution (MEA 5 mmol) was added to PHAD (0.74 g, 5 mmol), and the mixture was stirred for 12 h at room temperature, and a white precipitate was obtained. The precipitate collected by a filter was washed with DMAc and water for purification, then dried under vacuum followed by thermal imidization at 200 °C for 12 h under N_2.

3. Results and discussion

3.1. Polymer synthesis

The structures of model compound **2** were identified by far-IR and FT-IR spectra, as shown in Sup. 1a (Supporting information), characteristic peaks of the aromatic imide group were observed at ca. 1780 and 1719 cm^{-1} (asymmetric and symmetric stretching of imide C═O), ca. 1387 cm^{-1} (stretching of imide N and aromatic C), and ca. 717 cm^{-1} (deformation of imide). In addition, the peaks originating from the stretching of methylene are clearly observed at 3068 cm^{-1} and 2932 cm^{-1} for the MEA moiety, which indicates that MEAs were successfully reacted with the phthalic anhydride moiety. In far-IR spectrum (Sup. 1b) the ZnO particles exhibited a broad absorption band in the range of 400–550 cm^{-1}. The broad band can be also observed in model compound **2**, which indicates that ZnO particles exist in model **2**. In addition, the model **2** exhibits two characteristic peaks at around 530 cm^{-1} and 350 cm^{-1} which are assignable to the C–H stretching of benzene and C–N stretching of the imide linkage, respectively. These facts indicate the formation of model **2**.

The synthetic route is shown in Scheme 1. Here, we give an image for a relatively globular ball like structure for the HBPI according to previous reports [16,21], though we paid much more attention to the large amounts of terminal groups located at the peripherals of HBPI, and almost all the terminal groups in HBPI are functionalized by phthalic anhydride groups. The *in situ* sol–gel polymerization technique of the precursors of ZnO in the presence of MEA was first developed for the synthesis of poly(methyl methacrylate)/ZnO hybrids by Kim et al. [24]. In this study, difunctional MEA was also chosen as the coupling agent to terminate the anhydride end-groups of HBPIs and a chemical binder (coupling agent) to the surface of the ZnO nanoparticles. An MEA-Zn^{2+} solution was added to a poly(amic acid) (PAA) solution, the amino groups of MEA react with the peripheral anhydride terminals of HBPI and form stable covalent bonds. In addition, the hydroxyl group of MEA also joins in the successive sol–gel hydrolysis reactions of Zn^{2+}. Accompanied by the formation of ZnO, stable covalent bonds could be formed between the ZnO nanoparticles and MEA, and the thermal imidization of HBPIs was successively completed. After these processes, transparent ZnO/MEA/HBPIs hybrid films were obtained with a high-performance polymer matrix and high content of ZnO nanoparticles (above 10 wt%). The structures of HBPIs were identified by FT-IR spectra, as shown in Fig. 1, in which the characteristic peaks of the aromatic imide moiety were observed at ca. 1780 and 1719 cm^{-1} (asymmetric and symmetric stretching of imide C═O), and ca. 1387 cm^{-1} (stretching of imide N and aromatic C). The peaks originating from the terminal anhydride groups are clearly observed at 1850 cm^{-1} for a pristine HBPI and a physical blend film prepared by mixing

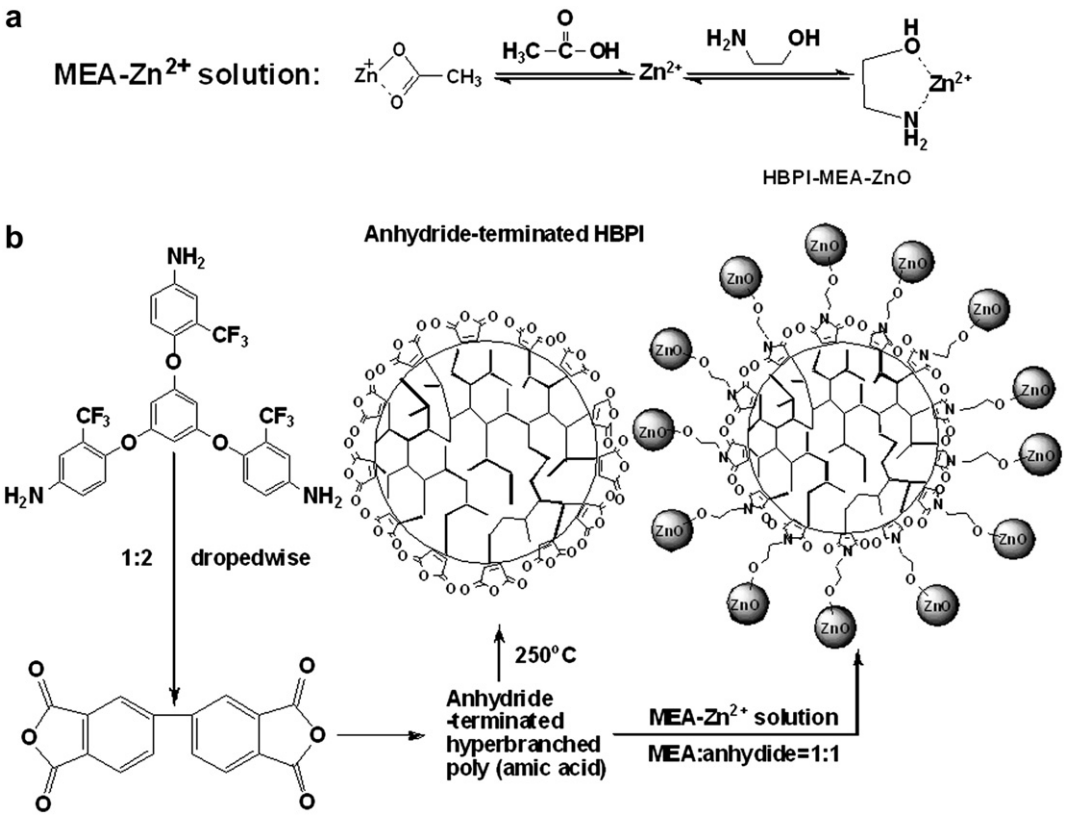

Scheme 1. (a) Sketch of the equilibria taking placing in the solutions. Three nucleophilic complexes (MEA, HO^- and CH_3COO^-) compete for the Zn^{2+} center; hydrolysis and condensation are spurred by temperature. (b) The synthesis route of pristine HBPI and HBPI-MEA-ZnO nanocomposites. ZnO nanoparticles were formed during thermal imidization.

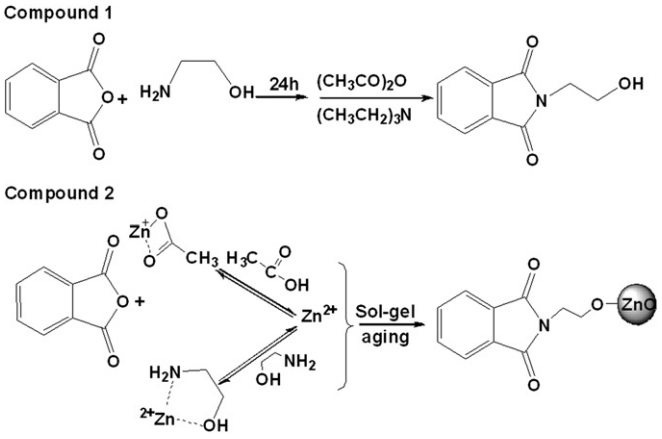

Scheme 2. Synthesis of model compounds **1** and **2**.

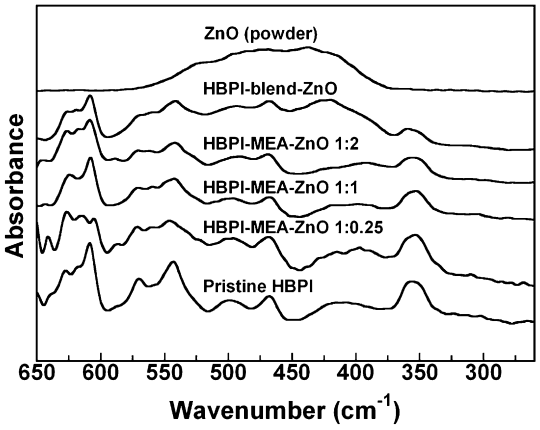

Fig. 2. Far-IR spectra of pristine HBPI and HBPI-MEA-ZnO hybrid films.

a PAA solution and sub-μm-size ZnO particles, followed by thermal curing (HBPI-blend-ZnO). In contrast, the peak disappeared after the treatment with MEA, which indicates that the anhydride terminals were successfully modified. The far-IR spectra of these films are shown in Fig. 2 with that of sub-μm size ZnO particles. The pristine HBPI exhibits five characteristic peaks at around 625, 570, 530, 470 and 350 cm^{-1}, which are assignable to the C=O stretching, CF_3-stretching, C–H stretching of benzene, –O– stretching and C–N stretching of the imide linkage, respectively. The ZnO particles precipitated in the films exhibited a broad absorption band in the range of 400–550 cm^{-1}. Compared to the blend film, all the *in situ* hybrid films (HBPI-MEA-ZnO) exhibited spectra similar to that of HBPI film, and absorptions from ZnO particles were not clearly observed. Kim et al. [24], illustrated the chemical structure of ZnO near the coupling points with MEA as a pseudo linear chain. As long as the ZnO chains are short enough and do not form crystalline domains, most of the ZnO nanoparticles are considered to exist in the amorphous state. The WAXD patterns also show that the *in situ* hybrid films and HBPI film exhibit no diffraction peaks except for amorphous halos (Fig. 3). In contrast, a broad diffraction halo from the amorphous HBPI component (10–30°) and sharp peaks from the crystalline ZnO were observed in the pattern of the blend film, which clearly indicates that two phase structures exist in the blend film. In contrast, a homogeneous phase structure was formed in the *in situ* hybrid films, and the broad amorphous halos observed in the WAXD patterns were gradually shifted to higher degrees by increasing the ZnO content. The mean intermolecular distances estimated from the peak maxima were 4.66 Å for the pristine HBPI, and 4.48, 4.16 and 4.01 Å for the HBPI-MEA-ZnO films, respectively. The gradual decrease in the intermolecular distances caused by the incorporation of ZnO is attributable to the densification of chain packing among the PI chains and ZnO nanoparticles owing to the covalent bonds and enhanced intermolecular interaction at PI–ZnO surfaces.

The TGA analysis curves measured in nitrogen and air are presented in Fig. 4(a) and (b), respectively. The *in situ* hybridized HBPI-MEA-ZnO films show lower decomposition temperatures than the pristine HBPI matrix, which could be ascribed to the aliphatic MEA segment. However, all the films prepared in this study exhibited good thermal stability with decomposition temperatures higher than 320 °C. Furthermore, the ZnO content was evaluated from the residual weights after curing at 900 °C in air. As presented in Fig. 4 (b), the residues of the hybrid films at 650 °C are in the range of 1.5–10.3% and increase by increasing the Zn^{2+} content in the MEA-Zn^{2+} solution. These char yields were in accordance with the expected weight fractions of inorganic ZnO content in the films. It was indicated that the ZnO particles were successfully incorporated into the HBPI matrices. Fig. 5 shows the DSC curves of the pristine HBPI and HBPI-MEA-ZnO films. The HBPI film exhibited a glass transition (T_g) at about 245 °C, whereas no apparent transition was observed for HBPI-MEA-ZnO films below 300 °C. We also used thermal mechanical analysis (TMA) to measure the glass transition

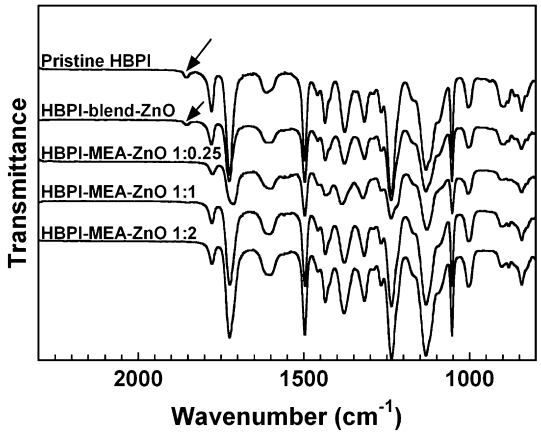

Fig. 1. FT-IR spectra of pristine HBPI and HBPI-MEA-ZnO hybrid films with different ZnO content.

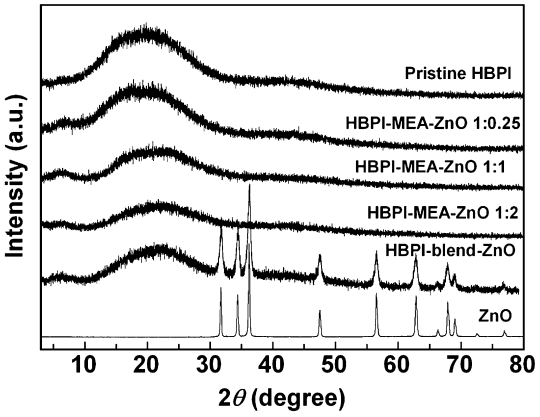

Fig. 3. Wide-angle X-ray diffraction patterns of pristine HBPI and HBP-MEA-ZnO hybrid films.

behavior of the hybrid films. A significant increase in T_g with the incorporation of ZnO was observed in the TMA curves. As shown in Fig. 6, the T_g of HBPI was 233 °C, and by increasing the content of ZnO, the T_gs were increased by as much as 80 °C. Further, no apparent glass transition was observed for HBPI-MEA-ZnO 1:2 below 350 °C, and thermal elongation of the HBPI film at elevated temperatures was effectively suppressed. This indicates that ZnO nanoparticles chemically bonded via MEA significantly restrict the mobility of the HBPI chains, and the T_g of the hybrid films approached their decomposition temperatures. Thermal analyses of the *in situ* hybrid films indicated that the ZnO nanoparticles were tightly bonded to the HBPI matrix and then exhibited good thermal stability.

Fig. 7(a) and (b) represents the TEM micrograph and EDS pattern of HBPI-MEA-ZnO 1:2 film. The TEM image shows a uniform surface without noticeable microstructures or significant ZnO aggregates. In addition, the homogeneity at the surface of the hybrid film can also be confirmed by the transparency from the photo image (listed inside the UV–vis spectra (Fig. 8)). In addition, distinct signals from Zn and O atoms were observed in the EDS pattern, whose positions agree well with the reference data [25].

3.2. Optical properties

Fig. 8 illustrates the UV–vis absorption spectra of HBPI and HBPI-MEA-ZnO films with thicknesses of ca. 20 μm. All the films exhibited good optical transparency in the range of 450–800 nm, which indicates that the average particle size of ZnO is significantly smaller than the wavelengths of visible light, and the particles are homogeneously dispersed in the HBPI-MEA-ZnO films. Since the absorption edge of ZnO is located at 388 nm [26], the slight contribution of the ZnO absorbance was observed as longer wavelength shifts of the absorption edges by increasing the concentration of ZnO.

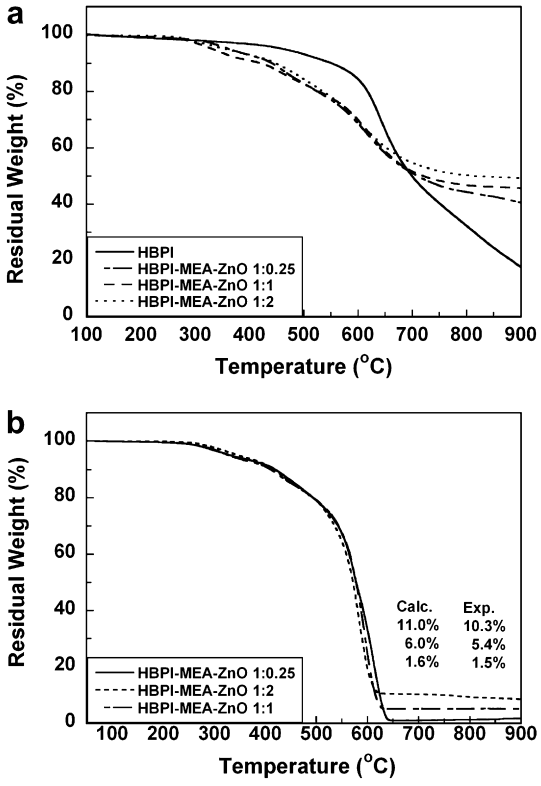

Fig. 4. TGA curves of pristine HBPI and HBPI-MEA-ZnO hybrid films measured (a) under nitrogen and (b) in air.

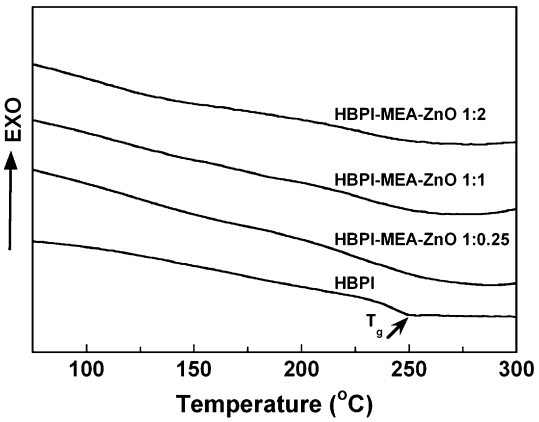

Fig. 5. DSC curves of pristine HBPI and HBPI-MEA-ZnO hybrid films.

3.3. Fluorescence of HBPI-MEA-ZnO nanohybrids

Figs. 9 and 10 illustrate the fluorescent excitation and emission spectra of the HBPI, HBPI-blend-ZnO, and HBPI-MEA-ZnO films with different ZnO content. The wavelengths of the fluorescence peaks are summarized in Table 1. It has been reported that two kinds of optical absorption bands are observed in conventional aromatic PI [27,28]. The first one is "locally excited" (LE) transition that occurs between two adjacent dianhydride moieties. The second one is "charge-transfer" (CT) transition originating from the CT complexes formed between electron-donating diamine and electron-accepting dianhydride moieties. The intra- and inter-molecular CT complexes can be formed in aromatic PIs. Hasegawa and coworkers reported that poly(*p*-phenylene biphenyltetracarboximide) (BPDA/PDA) exhibited a CT fluorescence with excitation wavelengths at around 340 and 400 nm. The former is assignable to the LE transition at the BPDA moiety followed by energy transfer from the excited LE (LE^*) to the excited CT (CT^*) state and successive emission to the ground CT state. On the other hand, the latter is assigned to direct excitation to the CT^* state followed by emission to the ground CT state [28]. As shown in the fluorescence spectra (Figs. 9 and 10), the pristine HBPI showed two excitation peaks at 344 and 434 nm with one emission peak at 500 nm. Hereafter, fluorescence peak positions will be expressed as $(\lambda_{ex} - \lambda_{em}) = (344/500\ \text{nm})$ and $(434/500\ \text{nm})$. This fluorescent behavior of HBPI is similar to the case of BPDA/PDA, and the photophysical process supposed for the pristine HBPI is illustrated in Fig. 12(a). The fluorescence peaks at (344/500 nm) and

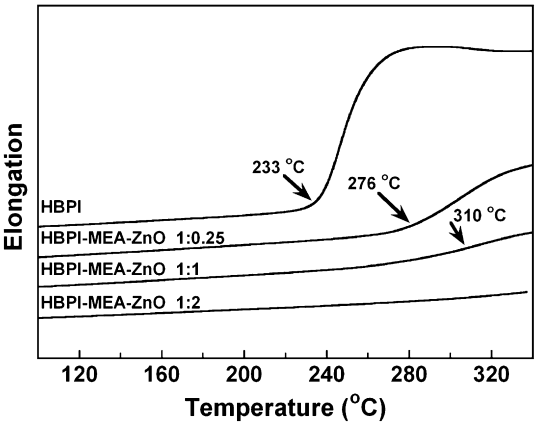

Fig. 6. TMA curves of pristine HBPI and HBPI-MEA-ZnO hybrid films. The glass transition temperatures are indicated by arrows.

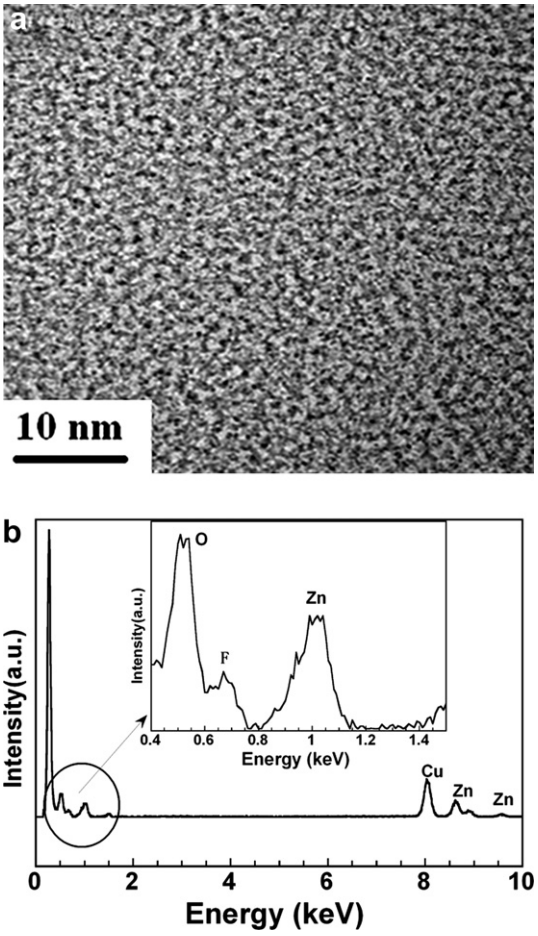

Fig. 7. (a) TEM micrographs and (b) EDS pattern of HBPI-MEA-ZnO 1:2. The region of interest in (b) is enlarged in the inset.

(434/500 nm) of HBPI are assignable to the CT emission via energy transfer from the LE* to the CT* state and direct CT excitation/emission, respectively.

On the other hand, the HBPI-blend-ZnO exhibited two fluorescence peaks at (344/480 nm) and (430/480 nm). The higher emission intensity of this film was caused by the significant light scattering by ZnO particles because only this film was translucent, whereas the other films were transparent. The center of the emission peak is located at around 480 nm, and two shoulder peaks

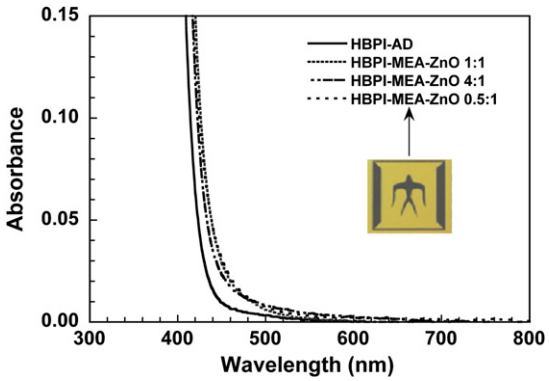

Fig. 8. UV–vis absorption spectra of the hybrid films formed on fused silica substrates. The inset is a photo of an HBPI-MEA-ZnO 1:2 hybrid film.

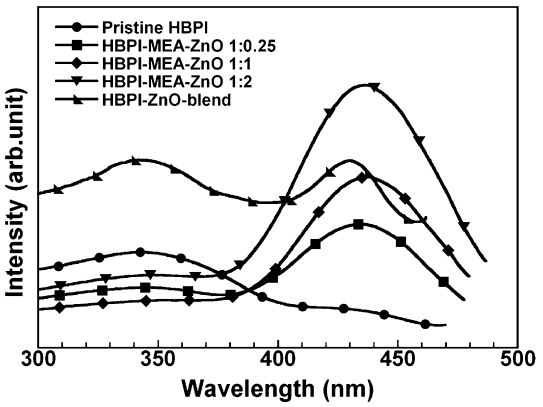

Fig. 9. Excitation spectra of pristine HBPI matrix, HBPI-MEA-ZnO hybrid films, and HBPI-blend-ZnO film.

are observed at around 470 and 500 nm. The spectral shapes of the emissions were not influenced by the excitation wavelengths. Similar fluorescence peaks were observed at (340/400, 470 and 515 nm), (430/470 nm) and (463/515 nm) for powdery ZnO (see Fig. 13). The series of peaks have been assigned to the surface defect emissions of ZnO [29], in which efficient energy transfer occurs between different defect levels. According to the Förster theory for Coulombic energy transfer, the overlap between the emission spectrum of an electron-donor and the absorption spectrum of an electron-acceptor causes effective intermolecular energy transfer. However, in this blend system, although the emission spectrum of

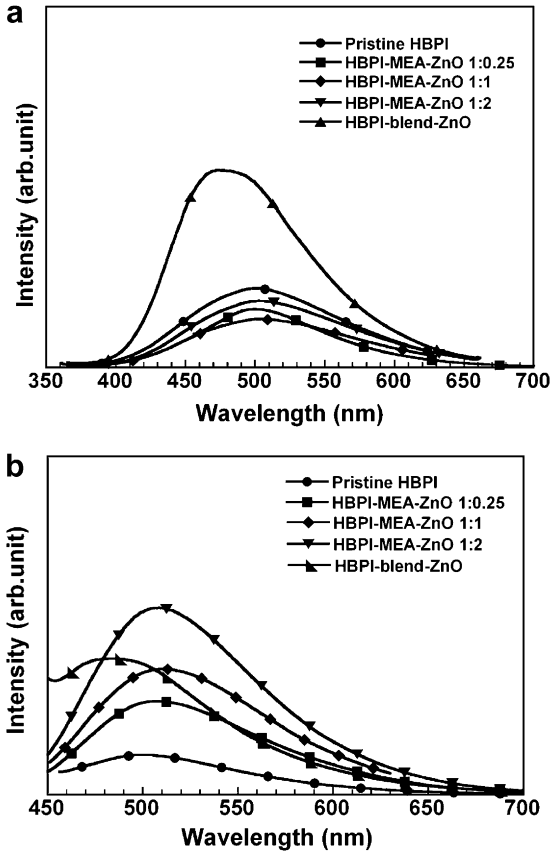

Fig. 10. Emission spectra of pristine HBPI and hybrid films: (a) $\lambda_{ex} \approx 340$ nm, (b) $\lambda_{ex} \approx 430$ nm.

Table 1
Wavelengths of the fluorescent excitation (λex)/emission (λem) peaks of all the materials.

	Sample				
	Pristine HBPI	BPDA-MEA ZnO	BPDA-blend-ZnO	ZnO	Compound **2**
$\lambda_{ex}/\lambda_{em}$ (nm/nm)	344/500	344/500	344/480	340/400, 470,515	380/460
	434/500	434/510	430/480	430/470 463/515	

ZnO overlaps with the absorption spectrum of the HBPI matrix, effective energy transfer did not occur from ZnO particles to HBPI chains. This is supported by the presence of ZnO emission in the fluorescence spectrum of HBPI-blend-ZnO. This fact clearly indicates that the average separation distance between the ZnO particles and HBPI chains was not sufficiently small for energy transfer, for which the typical critical separation is in the range of 7–40 Å. As seen in Fig. 9, the relative intensity of the peak at around 430 nm to that at around 340 nm for HBPI-blend-ZnO is higher than that of the pristine HBPI, which is due to the fluorescence of ZnO. The inferred photophysical process is illustrated in Fig. 12(b). When HBPI-blend-ZnO is excited at 344 nm and 430 nm, the ZnO particles and HBPI matrix should be independently excited, and they should obey the inherent routes for fluorescent emission without energy transfer to each other. The emission mechanism in this system can be explained as a simple superposition of the fluorescence from two independent components (the ZnO particles and HBPI chains).

As shown in Figs. 9 and 10, the fluorescence spectra of *in situ* hybrid films (HBPI-MEA-ZnO) are totally different from those of the pristine HBPI and HBPI-blend-ZnO films. In these hybrid films, energy transfer from the LE^* to CT^* state is no longer effective. The excitation peaks for the LE transition at 344 nm were decreased by increasing the ZnO content, whereas the excitation peaks for the CT transition at 434 nm were significantly increased in reverse. In addition, the corresponding CT emission intensity at 510 nm was increased when excited at the maximum absorption (434 nm). These facts clearly indicate the proximity of location and strong interactions between the ZnO nanoparticles and HBPI chains.

To confirm the fluorescence mechanism in the HBPI-MEA-ZnO hybrid system, two types of model compounds without (model **1**) and with ZnO (model **2**) were prepared (see Scheme 2). As shown in Fig. 11, model **2** exhibits fluorescence peaks at (380/460 nm), while no clear peak was observed in model **1**. Since the peak position and intensity of mode **2** are remarkably different from those of model **1**, the fluorescence of model **2** should originate from the surface defects of the ZnO bonded to phthalimide via MEA. In contrast to

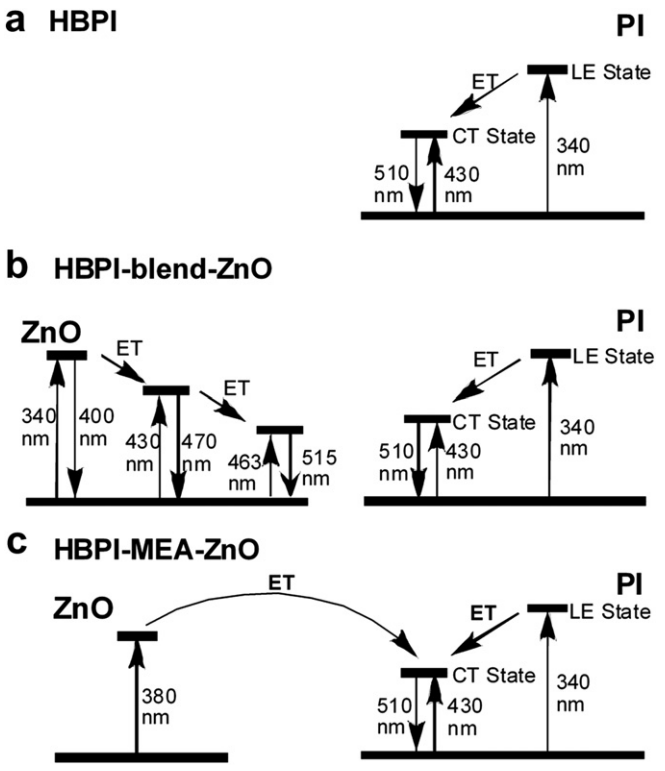

Fig. 12. Schematic photophysical processes: (a) pristine HBPI (b) HBPI-blend-ZnO (c) HBPI-MEA-ZnO.

HBPI-blend-ZnO film, emission peaks from ZnO particles were not clearly observed for HBPI-MEA-ZnO films, and the observed fluorescence is essentially attributed to the CT emission from HBPI. These facts clearly indicate that effective energy transfer from the surfaces of ZnO to HBPI chains occurred in the *in situ* hybrid films. ZnO nanoparticles are covalently bound to the termini of the HBPI chain, thus the average separation distance between these two components should be smaller than or comparable to the critical distance for effective energy transfer. As shown in Fig. 9, this unique energy transfer mechanism enhanced the CT excitation intensity (430 nm) by increasing the ZnO content. In contrast, CT emission with LE excitation at 340 nm did not show remarkable change by the *in situ* hybridization of HBPI with ZnO (see Figs. 9 and 10(a)). This indicates that ZnO in HBPI-MEA-ZnO films does not influence CT fluorescence with excitation at 340 nm. The photophysical process proposed for the *in situ* hybrid films is illustrated in Fig. 12

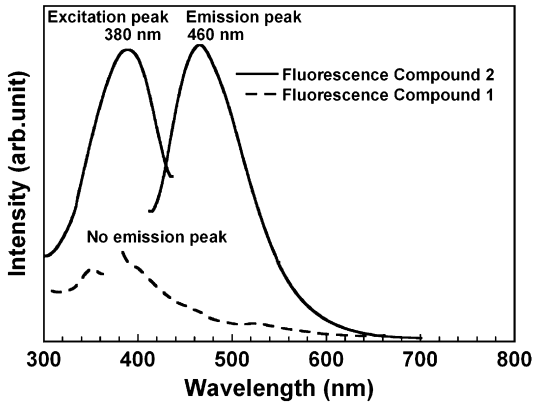

Fig. 11. Fluorescence excitation/emission spectra of model compounds **1** and **2**.

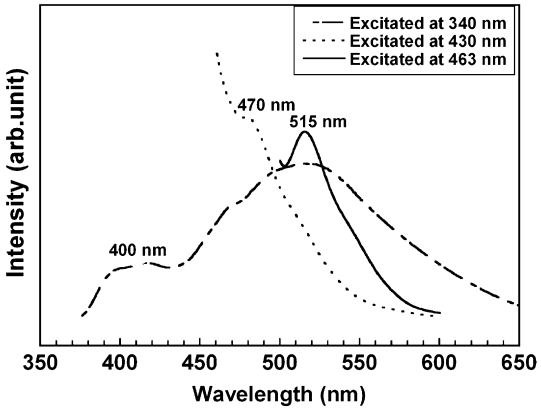

Fig. 13. Emission spectra of ZnO particles.

(c). When the films were excited at 344 nm, the same emission mechanism as that for pristine HBPI was exerted, and thus a CT emission peak at 500 nm was observed. In contrast, after being excited at 436 nm, the electronic energy generated near the surface of ZnO was effectively transferred via spatial migration to the CT^* state of the neighboring HBPI host. Consequently, a relatively strong CT fluorescence was obtained in the *in situ* hybrid HBPI-MEA-ZnO system. In summary, the combination of an HBPI having many anhydride termini and ZnO nanoparticles synthesized by the sol–gel method effectively shortened the distance between the light absorber (ZnO) to the light emitter (HBPI). In other words, the covalently bonded functional ZnO nanoparticles located in proximity to the HBPI chains effectively absorb radiation for excitation and transfer the generated energy to the HBPI matrix. The inorganic ZnO/organic HBPI hybrid system developed in this study can afford novel fluorescence emitting polymers with high thermal stability, good flexibility, and high transparency. The photophysical processes clarified for the *in situ* hybrid films will provide new materials for further applications and may open an interesting area for fluorescence research.

4. Conclusions

Based on the advantage of the multi-functional terminal groups of the highly branched chemical structures of hyperbranched polyimides (HBPIs), ZnO nanoparticles generated via sol–gel reactions were covalently bonded to the HBPI matrix by a chemical grafting method using MEA. Homogeneous and transparent hybrid films were successfully obtained by the conventional *in situ* sol–gel polymerization technique, and the average size of the ZnO particles was significantly smaller than the wavelengths of visible light. According to the TEM micrograph, the average size was smaller than 10 nm. By comparison with the pristine HBPI and physically blended films (HBPI-blend-ZnO), the fluorescence excitation and emission mechanisms of the *in situ* hybrid film (HBPI-MEA-ZnO) were clarified. An efficient energy transfer from the excited donor (ZnO) to the accepter (HBPI) occurred in this unique hybrid system, which originated from the sufficiently short distances between the ZnO surface and HBPI chains. The use of HBPI with many peripheral termini is an effective way to strengthen the interactions between inorganic nanoparticles and functional polymers. Compared to a physical blend of ZnO nanoparticles and a PI matrix, our method endows novel ZnO/HBPI hybrid materials with unique photophysical processes for fluorescence, which provides better potential materials for future fluorescence applications.

Acknowledgments

The authors sincerely thank Jun Koki and Katsuaki Hori at the center of advanced materials analysis in Tokyo Institute of Technology for the assistance of measurements of TEM.

Supplementary data

Supplementary data associated with this article can be found in the online version of this paper at doi:10.1016/j.polymer.2010.05.019.

References

[1] Colvin VL, Schlamp MC, Alivisator AP. Nature 1994;370:354.
[2] Dabbousi BO, Bawendi MG, Onitsukaa O, Rubner MF. Appl Phys Lett 1995;66:1316.
[3] Tessler N, Medvedev V, Kazes M, Kan S, Banin U. Science 2002;295:1506.
[4] Coe S, Woo WK, Bawendi M, Bulovic V. Nature (London) 2002;420:800.
[5] Huynh WU, Dittmer JJ, Alivisatos AP. Phys Rev B 1996;54:17628.
[6] Sage L. Anal Chem 2004;76:453A.
[7] Ajayan PM, Schadler LS, Braur PV. Nanocomposite science and technology. Weinheim: Wiley-VCH; 2003.
[8] Wang X, Zhou J, Lao C, Song J, Xu N, Wang ZL. Adv Mater 2008;19:1627.
[9] Dorfman A, Kumar N, Hahm L. Adv Mater 2006;18:2685.
[10] Bao J, Zimmler MA, Capasso F. Nano Lett 2006;6:1719.
[11] Hsu SC, Whang WT, Hung CH, Chiang PC, Hsiao YN. Macromol Chem Phys 2005;206:291.
[12] Hung CH, Whang WT. J Mater Chem 2005;15:267.
[13] Yuwono AH, Liu B, Xue J, Wang J, Elim HI, Ji W, et al. J Mater Chem 2004;14:2978.
[14] Su HW, Chen WC. J Mater Chem 2008;18:1139.
[15] Suzuki T, Yamada Y, Tsujita Y. Polymer 2004;45:7167.
[16] Fang JH, Kita H, Okamoto K. J Membr Sci 2001;182:245.
[17] Kim YH. J Polym Sci Part A Polym Chem 1998;36:1685.
[18] Voit BJ. J Polym Sci Part A Polym Chem 2000;38:2505.
[19] Inoue K. Prog Polym Sci 2000;25:453.
[20] Gao H, Wang D, Guan SW, Jiang W, Jiang ZH, Gao WN, et al. Macromol. Rapid Commun 2007;28:252.
[21] Gao H, Yan CQ, Guan SW, Jiang ZH. Polymer 2010;51:694.
[22] Chen H, Yin J. J Polym Sci Part A Polym Chem 2002;40:3804.
[23] Znaidi L, SolerIIlia GJAA, Benyahia S, Sanchez C, Kanaev AV. Thin Solid Film 2003;428:257.
[24] Li SH, Toprak MS, Jo YS, Dobson J, Kim DK, Muhammed M. Adv Mater 2007;19:4347.
[25] Gautam UK, Panchakarla LS, Dierre B, Fang XS, Bando Y, Sekiguchi T, et al. Adv Funct Mater 2009;19:131.
[26] Althues H, Henle J, Kaskel S. Chem Soc Rev 2007;36:1454.
[27] Hasegawa M, Shindo Y, Sugimura T, Ohshima S, Horie K, Kochi M, et al. J Polym Sci Part B Polym Phys 1993;31:1617.
[28] Hasegawa M, Horie K. Prog Polym Sci 2001;26:259.
[29] Aleksandra BD, Leung YH. Small 2006;8–9:944.